Ceramics International 50 (2024) 48988–48994

Contents lists available at ScienceDirect

Ceramics International

journal homepage: www.elsevier.com/locate/ceramint

Ce-doped magnesium borate glass-ceramic for optically stimulated luminescence dosimetry

D.A.A. de Vasconcelos [a,*], M.L. Souza [b], I.S. Silveira [a], E.D. Zanotto [b], L.V.E. Caldas [a]

[a] Nuclear and Energy Research Institute, National Nuclear Energy Commission – IPEN/CNEN, São Paulo, SP, Brazil
[b] Federal University of São Carlos, Graduate Program in Materials Science and Engineering, São Carlos, SP, Brazil

ARTICLE INFO

Keywords:
Optically stimulated luminescence
Magnesium borate
Cerium
Glass
Glass-ceramics

ABSTRACT

Despite intensive research in optically stimulated luminescence (OSL) dosimetry, the number of materials with suitable properties for practical application remains limited. Among these, magnesium tetraborate (MgB_4O_7) has attracted attention as a potential host because of its effective atomic number, similar to those of water and living tissues, and the possibility of producing neutron-sensitive material by controlling the content of the ^{10}B isotope. Specifically, Ce-doped MgB_4O_7 has been proposed as a promising OSL material for 2D dosimetry because of its rapid luminescence. While the literature on polycrystalline sintered MgB_4O_7:Ce is extensive, the objective of this work is to produce this material in *glass-ceramic* form, offering many advantages such as excellent formability into complex shapes, rapid mass production, easily controlled microstructure, and higher density (zero porosity) compared to conventional powder-sintered materials, potentially leading to dosimetric improvements. This paper describes the synthesis route and the effects of various thermal treatments of magnesium borate glass and the resulting glass-ceramics, along with their fundamental dosimetric properties. The samples heat-treated at 814 °C for 3 h (GC814) exhibited the most intense and stable thermoluminescence peaks, accounting for their lowest signal fading among the investigated treatment conditions. However, during the OSL readout, diminished intensity was observed. Analysis of the GC814 emission spectrum revealed TL peaks predominantly outside the used optical filter's primary transmittance range, likely contributing to the OSL signal reduction. Regardless of the thermal-treatment condition, all the samples presented excellent repeatability of the OSL response, with standard deviations ranging from 0.1 % to 0.7 %, underscoring the advantages of glass-ceramics over sintered ceramics. From step-annealing analysis, an optimal preheat treatment temperature was identified, and the activation energy of the three main peaks was determined. The encouraging results indicate the potential of this glass-ceramic as a practical OSL dosimeter and justify further investigation to optimize its OSL properties.

1. Introduction

Over the past decades, the refinement of modern three-dimensional radiotherapy techniques, such as Intensity Modulated Radiotherapy (IMRT), Stereotactic Radiosurgery (SRS), Stereotactic Ablative Radiation Therapy (SABR), and Volumetric Modulated Arc Therapy (VMAT), has enabled the delivery of very high doses to complex planning target volumes. As a result, there is a vital need for comprehensive spatially resolved measurements of delivered dose distributions to ensure the safety and accuracy of treatment plans for patients. These detectors require high spatial resolution, accounting for the steep gradient of the radiation field and beam alignment, and good energy dependence, to address volume averaging effects, lack of charged particle equilibrium, and partial occlusion of the radiation source [1].

Additionally, dosimetry in the presence of magnetic fields, such as those in Magnetic Resonance Imaging-Guided Radiation Therapy [2] and ultra-high dose rates of FLASH therapy [3], poses challenging aspects that are pushing the development of techniques capable of handling these extreme conditions [4]. The detectors currently implemented and studied have their limitations.

Among the alternative techniques being investigated, two-dimensional luminescence dosimetry, including techniques based on optically stimulated luminescence (OSL), thermoluminescence (TL), radioluminescence/scintillators (RL/SC), and radio-photoluminescence

* Corresponding author. Instituto de Pesquisas Energéticas e Nucleares (IPEN/CNEN), Av. Prof. Lineu Prestes, 2242 – Cidade Universitária, 05508-000, São Paulo, SP, Brazil.
E-mail address: azevedo.radiologia@gmail.com (D.A.A. de Vasconcelos).

https://doi.org/10.1016/j.ceramint.2024.09.231
Received 1 June 2024; Received in revised form 7 September 2024; Accepted 17 September 2024
Available online 18 September 2024

(RPL) [1,5–7], has been considered a promising candidate [7,8]. Each technique has its advantages and disadvantages, but the completely optical readout systems of RPL and OSL are particularly suited for developing measurement techniques in high dose-gradient fields [9,10] and benefit from the established technology of laser-scanning readout systems, widely used in computed radiography [11].

The phenomena of TL and OSL involve the emission of energy previously stored through the trapping of charged carriers, typically induced by exposure to ionizing or non-ionizing radiation. This stored energy is released in the form of light during thermal and optical stimulation, respectively. The fundamental theory of TL and OSL is based on the presence of imperfections, impurities, and defects within an otherwise ordered crystal lattice. These imperfections create discrete allowed energy levels within the forbidden energy gap, which are capable of capturing electrons or holes [12].

Moreover, OSL detectors may offer advantages such as independence from dose-rate and magnetic field effects. While Chen and Leung [13] theoretically predicted dose-rate dependence in TL and OSL detectors in a simplified model and under limited conditions, experimental data have shown the opposite [14–16]. Regarding magnetic fields, Spindeldreier et al. [17] reported a relatively small dose response decrease of −1.3 % per T (95 % confidence interval: 1.9 % to −0.7 %) and no significant angular dependence by the magnetic field for OSL detectors.

Despite these potential advantages, the number of materials suitable for practical application remains limited. For instance, the only two commercially available OSL materials, Al_2O_3:C and BeO, exhibit relevant drawbacks, such as a relatively low saturation limit [18] and long luminescence lifetime [19,20], hindering their use in high dose ranges and 2D dosimetry, respectively. These limitations further substantiate the need for new OSL materials.

Among the several new OSL materials investigated [21], magnesium tetraborate (MgB_4O_7) has attracted attention as a host material for dosimetry-based techniques like OSL and TL because of its effective atomic number ($Z_{eff} = 8.4$), similar to those of water ($Z_{eff} = 7.51$) and living tissues ($Z_{eff} = 7.35–7.65$), and the possibility of producing a neutron-sensitive material by controlling the host content of the ^{10}B isotope [22].

Gustafson et al. [23] determined the luminescence lifetime associated with the Ce^{3+} $5d \rightarrow 4f$ emission in polycrystalline MgB_4O_7 (31.5 ns), which is appropriate for laser scanning in imaging applications as this short lifetime prevents pixel bleeding [19], making its use for 2D dosimetry feasible. The Ce-doped MgB_4O_7 also presents a suitable trap depth for OSL dosimetry, with one strong TL glow peak at around 240 °C and two shoulder peaks: one at 170 °C and the other at 300 °C [24].

Although extensive literature exists on sintered Ce-doped [24–26], as well as co-doped with Gd, Na, and Li [27–29] magnesium tetraborate, to our knowledge, there are *no reports* on this material in glass-ceramic (GC) form. A MgB_4O_7:Ce GC could potentially have improved dosimetric properties because of its higher density and more uniform microstructure compared to conventional powder-sintered materials. Moreover, GC synthesis offers other advantages like good formability into complex shapes and rapid mass production, favorable for practical application and commercialization [29].

Therefore, the objective of this work is to demonstrate the feasibility of obtaining a MgB_4O_7:Ce glass-ceramic, and to investigate the optimal crystallization temperature and resulting microstructure to optimize its basic OSL dosimetric properties; a complete dosimetric characterization is beyond the scope of this study.

2. Materials and methods

2.1. Sample preparation

In theory, to obtain MgB_4O_7 phase crystals embedded in a residual glass matrix, the molar ratio between B_2O_3 and MgO should be approximately 2:1. However, evaporation of some boron during the melting process necessitates the use of higher proportions of this chemical element [29]. In practice, we produced a series of batches with varying concentrations of these precursors, including the Ce^{3+} dopant. Most as-made samples turned out to be partially or completely crystalized, rather than being glassy as expected.

Empirically, we found a suitable proportion of the Ce^{3+}-doped magnesium borate to be $55B_2O_3 – 45MgO – 0.3CeO_2$ (mol%), which was subsequently normalized to obtain 100 %. For production, the precursors MgO (Sigma-Aldrich, 99 %, source MKCR6037), B_2O_3 (Sigma Aldrich, 99.98 %, source MKCF9909), and CeO_2 (Sigma Aldrich, 99 %) were weighted and uniformly mixed in a high-speed mixer at 1200 rpm for 5 min. The mixture was then melted at ~1250 °C for 1 h in a platinum crucible. The final glass was obtained by pouring the melt and splat-cooling it between two steel plates, yielding glassy samples approximately 2.5 mm thick. Following the glass synthesis, both powder and small monoliths were prepared for further investigation. The powder was sieved to select grains of ~60 μm, while the as-made glass was cut using a diamond saw into 25 monoliths. These monoliths were then polished using sandpapers of 320, 400, 500, 600, and 1200 mesh, resulting in dimensions of approximately 5×5 mm^2 and a thickness of 0.6 mm.

To determine the optimal crystallization temperature for the best dosimetric properties of the material, five groups of five as-made glass monoliths were heat-treated at 630 °C, 676 °C, 722 °C, 768 °C, and 814 °C for 3 h. This was performed in an oven assembled at the Center for Research, Technology, and Education in Vitreous Materials (CeRTEV - Federal University of São Carlos, Brazil), which uses a ZAS (mullite-zirconia) internal tube and operates at temperatures up to (1100 ± 1) °C. The selected temperatures were based on the evaluation of the glass transition temperature (T_g) and the crystallization temperature (T_x), obtained from differential scanning calorimetry (DSC) using a Netzsch DSC 404 calorimeter. The measurement was performed on both powder (~32 mg) and monolith samples, with a heating profile starting from room temperature to 1100 °C, at a rate of 10 °C/min.

For simplicity, the GC samples of each group were named GC630, GC676, GC722, GC768, and GC814, corresponding to their thermal-treatment temperatures in Celsius degrees.

2.2. Characterization

The powders of the samples were used to determine the phase composition of the crystalline materials. This was performed utilizing an X-ray diffractometer, model Ultima IV RIGAKU, equipped with a CuK_α radiation ($\lambda = 1.54$ Å). The X-ray tube was operated at 40 kV and 20 mA, scanning in 2θ from 10 to 80°, with steps of 0.02°.s^{-1}, at room temperature. The X-ray diffractograms were then matched to patterns from the International Center for Diffraction Data (ICDD) PDF.

TL and OSL measurements were carried out using a Risø TL/OSL reader, model DA-20 (Risø National Laboratory, Denmark). OSL data were collected using a Hoya U-340 filter (7.0 mm thickness, transmission between 290 nm and 390 nm, Hoya Corp.), while no filter was used for the TL readouts, which were performed at a heating rate of 1 °C/s in the presence of N_2 to prevent oxidation and suppress spurious signals. No preheat treatment aimed at depleting the unstable peaks was conducted in any of the investigations. The irradiation procedure was conducted using a $^{90}Sr/^{90}Y$ beta source (0.08 Gy/s, in 2023) integrated into the reader, delivering a dose of 0.8 Gy to the samples for all investigations.

To obtain the TL emission spectrum, the photomultiplier was removed from the Risø system, and an optical fiber with a core diameter of 600 μm, connected to an Ocean Optics QE65 Pro spectrometer (operating in the 200–1000 nm range), was attached to the reader. The emission wavelength was measured by heating sample in a controlled manner up to 350 °C, at heating rate of 1 °C/s. Data were collected using the Spectra Suite software (Ocean Optics).

After irradiation, step-annealing analysis was performed by

preheating the sample (T_{stop}) between 50 °C and 350 °C in 10 °C increments, using a controlled heating rate of 1 °C/s until the desired temperature was reached, followed by cooling to room temperature. The TL measurements were then carried out.

3. Results and discussion

3.1. Thermal behavior of the as-made glass

The DSC curve of the as-made Ce-doped magnesium borate glass in both powder and monolith forms is shown in Fig. 1. The data indicate a glass transition at ~630 °C for both the powder (in red) and the monolith (in black). The notable difference of ~71 °C between the crystallization peak temperatures of the two curves suggests a dominant superficial crystallization process. This phenomenon indicates the material's outer layers are at a higher energetic level, due to incompletely fulfilled atomic bonds, making them more susceptible to crystallization. As a result, since the powder material has a larger surface area relative to the monolith, it exhibits a proportionally higher degree of crystallization. In general, the powder shows lower temperatures than the monolith, as observed in Fig. 1.

Although the melting temperatures are not influential for this study, it is important to emphasize its significant gap to the crystallization temperatures. This difference ensures a good margin for the samples to remain undeformed during the controlled crystallization processes.

For the GC processing, the transformation temperatures adopted are those of the monolith, namely $T_g = 630$ °C and $T_p = 814$ °C, as it is the form chosen for the intended applications.

3.2. Structural analysis

The XRD patterns of the GC samples for each thermal treatment are shown in Fig. 2. The patterns reveal that the samples subjected to 630 °C and 676 °C retained their amorphous glassy structure, while those exposed to 722 °C, 768 °C, and 814 °C were successfully crystallized.

The predominant phases of the crystalized samples are $Mg_2B_2O_5$ (PDF #86–531) and MgB_4O_7 (PDF #76–666), as identified in Fig. 2. The main distinction between these XRD patterns is the intensity variation of certain peaks relative to others. For example, with an increase in the crystallization temperature utilized, there is a noticeable rise in the intensity of certain MgB_4O_7 phase peaks, such as at 2θ ~17°, while the peak at 2θ = 35°, corresponding to the $Mg_2B_2O_5$ phase, decreases significantly. That suggests a formation preference of the MgB_4O_7 phase at higher temperatures.

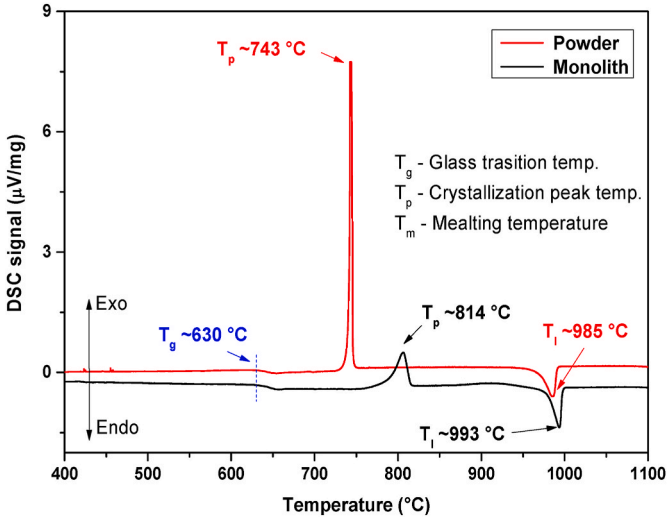

Fig. 1. DSC curve of the as-made glass in the powder and monolith forms.

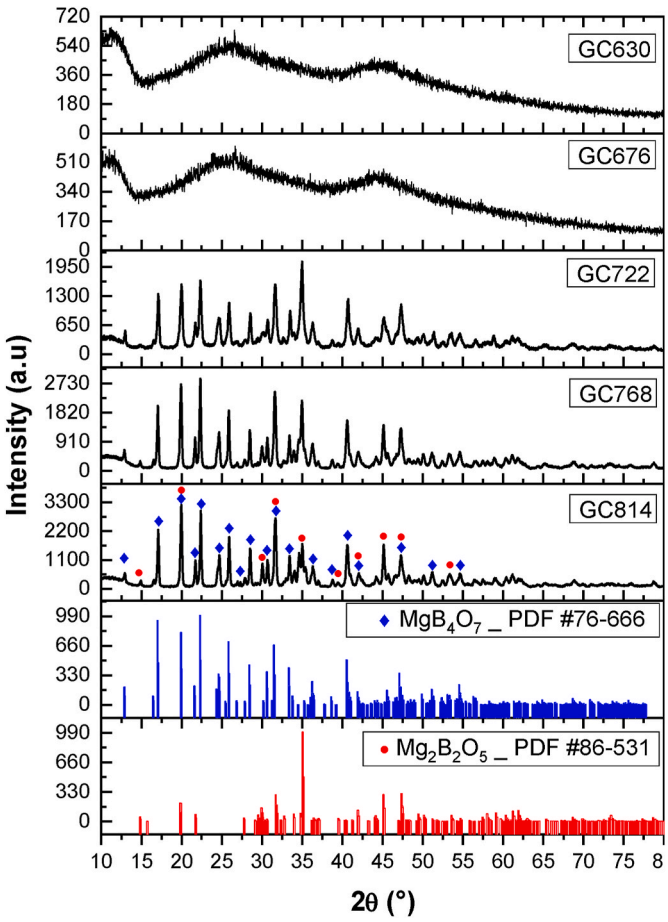

Fig. 2. XRD patterns of the prepared samples and b) reference data of the MgB_4O_7 (PDF #76–666) and $Mg_2B_2O_5$ (PDF #86–531) crystalline phases of the crystallized samples.

The conclusions drawn from the XRD pattern analysis can be qualitatively corroborated by the visual appearance of the thermally treated samples shown in Fig. 3, which exhibit a gradual increase in opacity, characteristic of the crystallization process.

3.3. Effect of thermal treatments

The effect of post-synthesis thermal treatments on the luminescence properties of the Ce-doped magnesium borate was investigated. Fig. 3 shows the TL glow curves of one GC sample from each treatment condition. As expected, the samples that retained a glass matrix presented a completely distinct curve shape, featuring one large peak (P1) with maximum intensity around 100 °C. This is similar to the MgB_4O_7 glass without any dopant, reported by Bakhsh et al. [30]. P1 is also observed in the curves of the crystallized samples but in a much smaller proportion. The higher crystallization temperatures tend to favor the MgB_4O_7 phase over the $Mg_2B_2O_5$ phase, which might explain the differences between the samples, particularly the GC722, which shows no P2 and

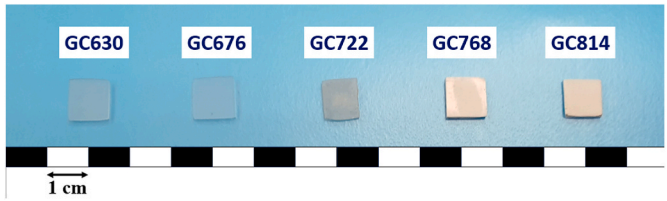

Fig. 3. Appearance of the samples for each treatment condition.

P4, in contrast to GC768 and GC814. This indicates that **a higher proportion of the MgB_4O_7 phase might be preferable for the dosimetric properties of the material.**

Regarding the shape of the GC722 TL glow curve, it closely resembles those reported by Kitagawa et al. [29], who investigated a magnesium borate glass-ceramic doped with cerium and lithium. In contrast, the GC768 and GC814 TL glow curves perfectly match that described by Dogan and Yazici [24] for their Ce-doped MgB_4O_7 produced by a "melting point method", resulting in a polycrystalline power.

In contrast to the behavior of the TL curves, the integral of the OSL curves decreased with increasing treatment temperature, as shown in Fig. 5. To investigate this trend, the emission spectrum of the GC814 sample was obtained. As shown in Fig. 6, the majority of the emission is concentrated in the red/infrared region, around 700 nm, suggesting that a significant portion of the emission is being blocked by the Hoya U-340 optical filter used during the measurements. This filter primarily transmits photons in the 290–390 nm range.

This loss of sensitivity can be totally or partially mitigated by replacing the optical filter with a more suitable option available for the equipment. The first option is the Schott BG3 filter, which exhibits nearly 1.0 transmittance for photons from 700 nm to 900 nm range, aligning with the emission spectrum of GC814. However, this filter also transmits photons in the blue region, necessitating the use of different stimulation LEDs to prevent damage to the photomultiplier. Additionally, the electron traps may not be responsive to the new stimulation LEDs. The second alternative is the Schott UG11 filter, which has a peak transmittance of approximately 0.3 in the infrared region at 720 nm – considerably lower than that of the first option – but allows for the continued use of blue stimulation LEDs. Since neither filter was available for the present study, the investigation proceeded with the Hoya U-340 filter.

To further investigate the reasons behind the decrease in OSL intensity, especially in GC814, which exhibited the greatest loss, we analyzed its TL curves before and after the OSL readout. The results, shown in Fig. 7, suggest that P4 is the only peak whose trapping centers are not emptied by the optical stimulation of blue LEDs. Since the emergence of P4 is directly related to the increased treatment temperature, this observation may provide an additional explanation for the loss of intensity from TL to OSL measurements.

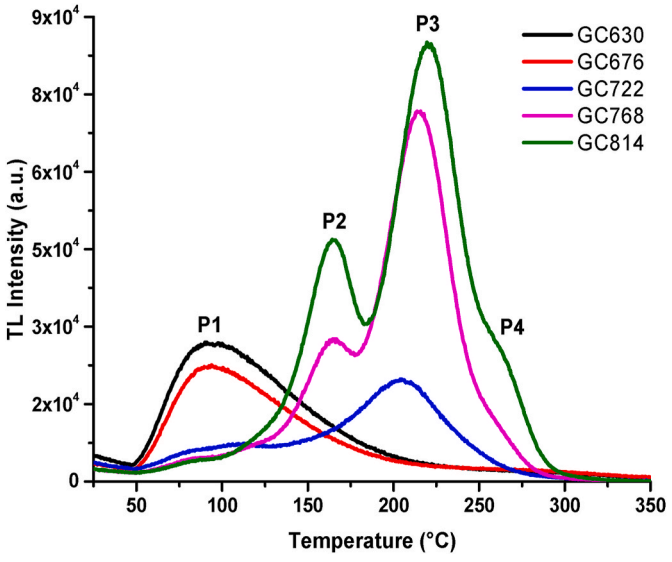

Fig. 4. TL glow curves of one GC sample of each thermal treatment, all normalized by the mass and with the apparent peaks indicated.

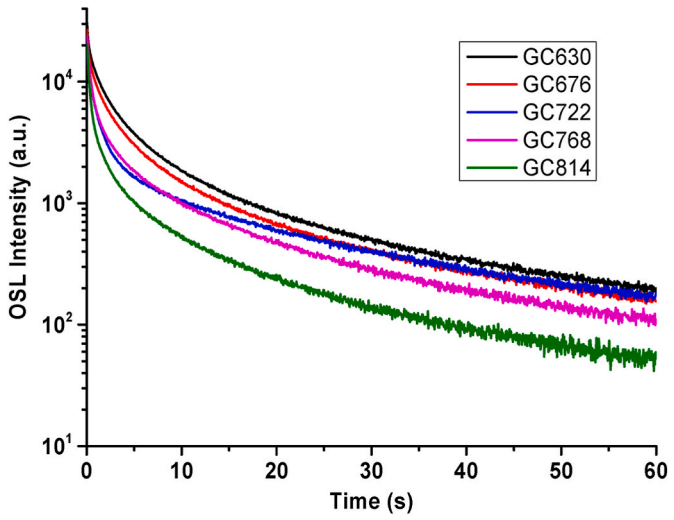

Fig. 5. OSL curves of one GC sample of each thermal treatment, all normalized by the mass and with the apparent peaks indicated.

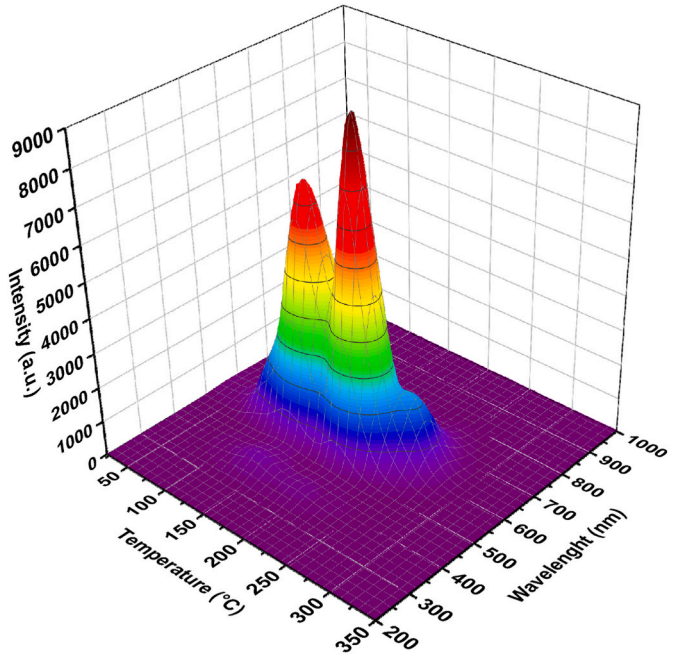

Fig. 6. Emission spectra of GC814.

3.4. OSL and TL fading

The total OSL fading curves for a sample of each treatment condition are presented in Fig. 8, where the OSL signal was plotted as a function of the delay time between irradiation and readout. As observed in Table 1, the GC630 and GC676 samples showed the highest intensities for readouts carried out immediately after the irradiation. However, because of their shallow electron trap nature, their signal drops steeply within a few minutes after irradiation, ultimately losing about 97 % of their initial intensity after a 360-min delay. The GC722 sample experienced a similar decline, although it displayed a peak at a higher temperature (Fig. 4). This might be attributed to its emission spectra, where the more stable peak is absorbed by the OSL filter, as previously suggested. This phenomenon also accounts for the lower initial intensities observed in the GC768 and GC814 samples compared to others.

The deep trap-related peaks in the GC768 and GC814 samples justify

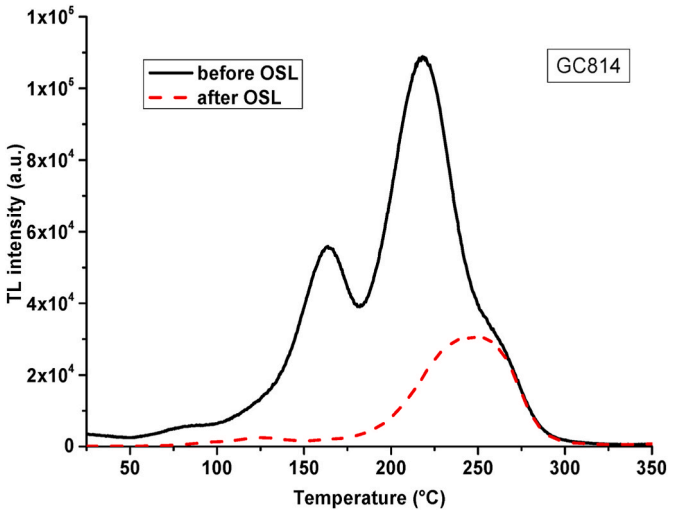

Fig. 7. Comparison between the TL of GC814 before and after OSL readout for 60 s. A heating rate of 1 °C/s was employed and no optical filter was used for the TL measurements.

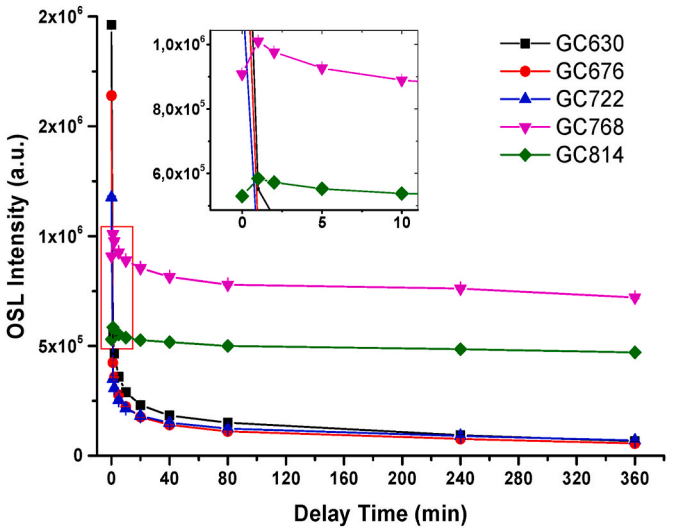

Fig. 8. OSL fading for samples of each treatment condition. Each data point represents the average and standard deviation of five measurements of a sample. The integral of the OSL curve was calculated subtracted from the readout of the respective non-irradiated sample and normalized by the average mass of all samples.

their much smaller fading over time, likely related to the less stable peaks P1 and P2. It is also noteworthy that for these two samples, which underwent higher thermal-treatment temperatures, there was a slight increase in intensity between the delay times of 0 and 1 min. This could indicate anomalous fading, possibly due to quantum tunneling [31]. However, this phenomenon is usually related to a decrease, not an increase, in signal intensity over time. Therefore, further investigation is required to understand the underlying mechanism more comprehensively.

The GC814 sample's characteristics, mainly its higher TL intensity and peaks at higher temperatures, which tend to be more stable over time, make it a favorable candidate for dosimetric applications compared to other samples with different treatment conditions. Thus, its TL fading was further investigated. The results, shown in Fig. 9, demonstrate the curve behavior over time, up to 360 min after irradiation and before readout. As expected, the shallow traps associated with P1 are responsible for the signal's disappearance after the investigated time, significantly reducing the intensity of P2. These are the two main factors behind the fading observed for the GC814 sample in Fig. 8, as P3 and P4 are associated with deep electron traps. The decrease in the maximum intensity of P3 is most likely a result of the diminishing tail of P2, as there is no change on the right side of P3, and it has been reported to be stable at that temperature [24,29].

The reduction of the area under the TL curves between the data related to the delay times of 0 and 360 min for the GC814 sample was approximately 16 %. For practical purposes, a pre-heat treatment can be carried out before the measurement to eliminate P1 and P2 peaks, focusing only on the stable peaks and thereby reducing material fading.

3.5. Repeatability of OSL response

The repeatability of the response of all 25 monoliths was evaluated, and the results are shown in Table 1. The data represent the average and standard deviation of five measurements of each sample irradiated with 0.8 Gy. The integral of the OSL curve was calculated, subtracted from the readout of the respective non-irradiated sample, and normalized by the average mass of all monoliths.

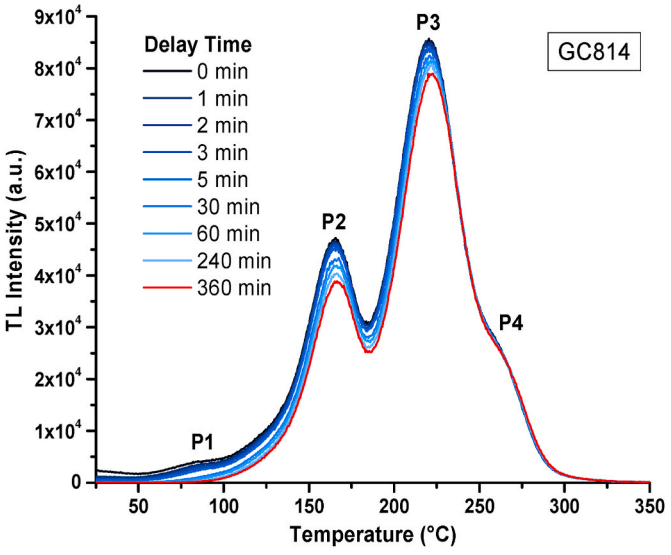

Fig. 9. TL curves with different delay times between the irradiation and the readout of the GC814 sample.

Table 1
Repeatability of the OSL response for all samples of each thermal-treatment condition (average of 5 measurements x10^6 - arbitrary units).

Samples	GC630		GC676		GC722		GC768		GC814	
	$\overline{X}$	S.D. (%)	$\overline{X}$	S.D. (%)	$\overline{X}$	S.D. (%)	$\overline{X}$	S.D. (%)	$\overline{X}$	S.D. (%)
1	1.65	0.48	1.63	0.41	1.07	0.51	0.91	0.14	0.53	0.18
2	1.45	0.20	1.95	0.67	0.95	0.36	0.84	0.57	0.41	0.34
3	1.54	0.39	1.64	0.46	0.98	0.70	1.01	0.29	0.57	0.71
4	1.67	0.47	1.35	0.21	1.10	0.43	0.95	0.28	0.37	0.31
5	1.55	0.23	1.60	0.25	0.87	0.65	0.98	0.16	0.42	0.32

Although the number of samples for each group was not designed to enable a full dosimetric characterization, it was still possible to identify some unique features of our material, such as the very low standard deviation, ranging from 0.1 to 0.7, for all samples, regardless of the structural differences due to the varying thermal-treatment temperatures. These figures ratify the potential of a properly conducted GC synthesis, rarely seen in the literature, as noted in a review by Oliveira et al. [32]. Such low standard deviations are advantageous for any application, but their importance is particularly pronounced in radiotherapy. However, further investigation is needed to confirm whether this level of repeatability is maintained at higher doses.

3.6. Step-annealing

To gain a deeper understanding of the thermal stability of the trapping centers and propose an appropriate preheat treatment to reduce fading due to shallow traps and enhance the repeatability and reproducibility of the GC814 samples, a step-annealing test was conducted. The glow curves corresponding to each step-annealing condition are shown in Fig. 10, along with the maximum TL intensity of each curve. As the preheat temperature increases, P1 begins depleting. However, because of its relatively small size compared to the other peaks, its fading has minimal impact on the overall integral of the glow curve, as indicated by the trend line associated with P1. At a preheat temperature of approximately 130 °C, P1 is fully depleted, and the electrons trapped in P2-related trap begin releasing, continuing up to a preheat temperature of around 190 °C. This is indicated by the green symbol and represents the suggested optimal preheat condition, effectively depleting the unstable traps without significantly affecting the stable ones (P3 and P4). P3 begins being impacted at temperatures of 200 °C and above, resulting in a sharp decrease in the integral of the glow curve, confirming this peak as the most intense. Unlike the other peaks, P4 does not exhibit linear depletion behavior, which will be discussed further in the subsequent analysis.

To extract the individual TL components of the glow curve and estimate the activation energy of the traps, the Repeated Initial Rise (RIR) method was applied. This method is widely used because its primary advantage is that it does not depend on the kinetics of the peaks. It is based on the assumption that variations in the concentration of charge carriers can be disregarded at temperatures below the maximum intensity temperature of the respective peak (T_m) [33]. This procedure allows for the adjustment of the equation $I(T) = C\exp(-E/kT)$ to determine the activation energies of this peak [34], where I is the TL glow curve intensity (a.u.), C is a constant, k is Boltzmann's constant, and E and T are the activation energy (eV) and temperature (K), respectively.

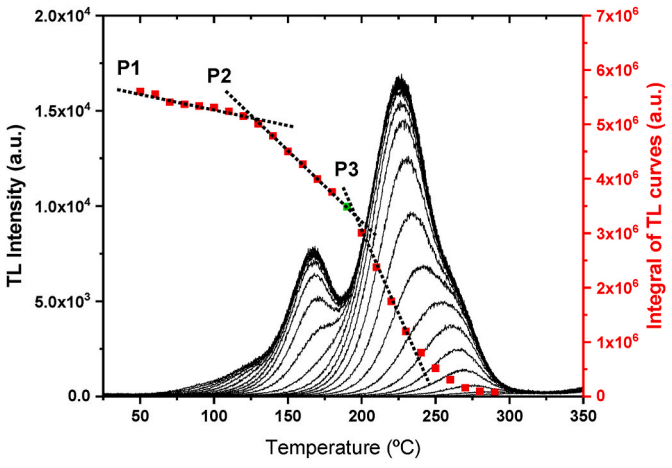

Fig. 10. Remanent TL curves after each preheat temperature of the step-annealing for the GC814 sample and the respective integral of each curve.

Fig. 11 shows the T_m-T_{stop} graphs, highlighting three distinct regions—E_1, E_2 and E_3—corresponding to the three main peaks, P2, P3 and P4, located at approximately 165 °C, 230 °C, and 260 °C, respectively. Because of the proportional size of P1 and its proximity to P2, it was not possible to distinguish them using preheats of steps of 10 °C.

The first two regions exhibit a plateau, indicative of a well-defined energy associated with first-order kinetics peaks. In contrast, the third region, related to P4, lacks a plateau, as also observed in Fig. 10 with its non-linear depletion. That behavior can be attributed to one of two possible explanations: either the dosimetric peak consists of several closely spaced first-order kinetics peaks, or it involves a complex structure that includes at least one peak with a kinetic order greater than one [35].

Table 2 summarizes the identified activation energies and their associated errors. Additionally, the intermediate points between regions 2 and 3, as depicted in Fig. 11, cannot be directly attributed to either P3 or P4, as the TL signal intensity was insufficient to produce statistically reliable data.

4. Summary and conclusions

In this study, we successfully produced Ce-doped magnesium borate glass-ceramics with a nominal composition of $55B_2O_3$ – 45MgO – $0.3CeO_2$ (mol%) through several thermal treatments. We verified the crystallization of glass samples subjected to three treatment temperatures, noting that some samples remained in their glassy state. The glass-ceramics exhibited two crystal phases, $Mg_2B_2O_5$ and MgB_4O_7, with the latter prevailing at higher crystallization temperatures.

Among all the treatment conditions investigated, the GC814 sample showed the most favorable dosimetric properties, characterized by intense and stable peaks. Nevertheless, analysis of its emission spectrum revealed that the peaks are predominantly in the red/infrared region, outside the primary transmittance range of the optical filter used. This, along with the presence of a peak that is non-optically sensitive to the LED stimulation, likely explains the significant reduction in its OSL signal – a limitation that could be mitigated by utilizing a more appropriate optical filter. Moreover, an important observation was the consistent repeatability of the OSL response across all glass and GC samples regardless of the thermal-treatment condition, with standard deviations ranging from 0.1 % to 0.7 %, ratifying the efficacy of the developed materials.

A more comprehensive understanding of the thermal stability of the

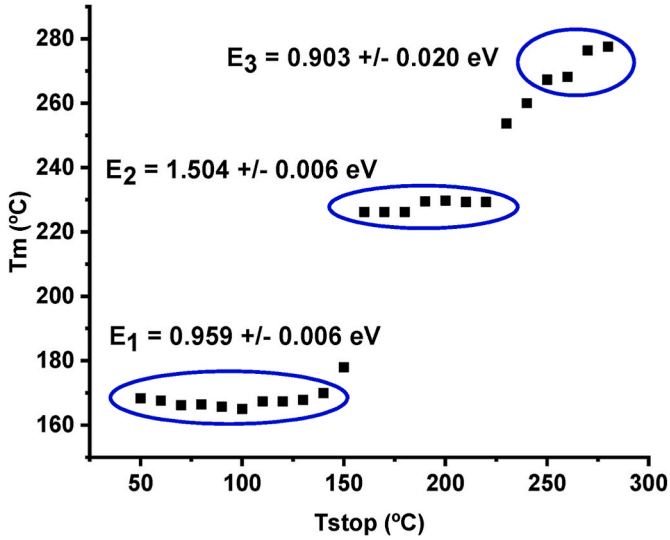

Fig. 11. The graph of T_m-T_{stop} for a GC814 sample.

Table 2
Activation energies (eV) obtained for each of the three regions, and their corresponding temperatures.

Peak	Region	Tstop (°C)	Tm (°C)	Activation Energy (eV)	Error (eV)
1	E_1	*	*	*	*
2		50–150	165	0.96	0.006
3	E_2	160–230	228	1.50	0.007
4	E_3	240–290	265	0.90	0.02

trapping centers was obtained through a step-annealing analysis, which, in conjunction with the Repeated Initial Rise method, enabled the determination of the activation energies of the three main peaks of the GC814 sample. The step-annealing data also allowed for the establishment of an optimal temperature for a preheat treatment designed to effectively deplete the unstable peaks. The presented positive results corroborate the potential of this material as a practical OSL dosimeter, which warrants further investigation to optimize the OSL properties.

CRediT authorship contribution statement

D.A.A. de Vasconcelos: Writing – review & editing, Writing – original draft, Validation, Resources, Methodology, Investigation, Funding acquisition, Formal analysis, Data curation, Conceptualization. **M.L. Souza:** Writing – review & editing, Visualization, Validation, Methodology, Investigation, Formal analysis, Data curation. **I.S. Silveira:** Writing – review & editing, Visualization, Validation, Methodology, Investigation, Formal analysis, Data curation. **E.D. Zanotto:** Writing – review & editing, Supervision, Resources, Methodology, Funding acquisition, Formal analysis. **L.V.E. Caldas:** Writing – review & editing, Supervision, Resources, Project administration, Methodology, Funding acquisition, Formal analysis.

Declaration of competing interest

The authors declare that they have no known competing financial interests or personal relationships that could have appeared to influence the work reported in this paper.

Acknowledgements

This study was supported by the Brazilian funding agencies FAPESP (grant nos. 2020/06268-9, 13/07793-6, and 2018/05982-0), CNPq (grant nos. 305142/2021-6 and 406303/2022-3), and CAPES (Finance Code 001).

References

[1] L. de Freitas Nascimento, F. Castellano, J. Goossens, A. van Dijk, P. Leblans, M. De Saint-Hubert, Investigation of 2D radiophotoluminescence films in radiotherapy: multileaf collimator Quality Assurance and small field dosimetry, Nucl. Instruments Methods Phys. Res. Sect. A Accel. Spectrometers, Detect. Assoc. Equip. 1028 (2022) 166349.
[2] D.J. O'Brien, N. Schupp, S. Pencea, J. Dolan, G.O. Sawakuchi, Dosimetry in the presence of strong magnetic fields, J. Phys. Conf. Ser. 847 (2017) 012055.
[3] F. Di Martino, P. Barca, S. Barone, E. Bortoli, R. Borgheresi, S. De Stefano, M. Di Francesco, L. Faillace, L. Grasso, L. Giuliano, S. Linsalata, D. Marfisi, M. Pacitti, M. Migliorati, G. Felici, L. Palumbo, FLASH radiotherapy with electrons: issues related to the production, monitoring, and dosimetric characterization of the beam, Front. Physiol. 8 (2020) 1–14.
[4] N. Shrestha, D. Vandenbroucke, P. Leblans, E.G. Yukihara, Feasibility studies on the use of MgB_4O_7:Ce,Li-based films in 2D optically stimulated luminescence dosimetry, Phys. Open 5 (2020) 100037.
[5] P. Olko, B. Marczewska, L. Czopyk, M.A. Czermak, M. Kłosowski, M.P. R. Waligórski, New 2-D dosimetric technique for radiotherapy based on planar thermoluminescent detectors, Radiat. Protect. Dosim. 118 (2006) 213–218.
[6] M. Guillot, L. Gingras, L. Archambault, S. Beddar, L. Beaulieu, Performance assessment of a 2D array of plastic scintillation detectors for IMRT quality assurance, Phys. Med. Biol. 58 (2013) 4439–4454.
[7] V. Vanreusel, A. Gasparini, F. Galante, G. Mariani, M. Pacitti, A. Colijn, B. Reniers, B. Yalvac, B. Vandenbroucke, M. Peeters, P. Leblans, G. Felici, D. Verellen, D.N. L. Freitas, Optically stimulated luminescence system as an alternative for radiochromic film for 2D reference dosimetry in UHDR electron beams, Phys. Med. 114 (2023) 103147.
[8] U. Jelen, J. Begg, Dosimetry needs for MRI-linacs, J. Phys. Conf. Ser. 1305 (2019) 012010.
[9] K. Idri, S. Member, L. Santoro, E. Charpiot, J. Herault, A. Costa, N. Aillères, R. Delard, J.R. Vaillé, J. Fesquet, L. Dusseau, S. Member, Quality control of intensity modulated radiation therapy with optically stimulated luminescent films, IEEE Trans. Nucl. Sci. 51 (2004) 3638–3641.
[10] L.F. Nascimento, W. Crijns, G. Goveia, Z. Mirotta, L.F. Souza, F. Vanhavere, C. Saldarriaga Vargas, M. De Saint-Hubert, 2D reader for dose mapping in radiotherapy using radiophotoluminescent films, Radiat. Meas. 129 (2019) 106202.
[11] J.A. Rowlands, The physics of computed radiography, Phys. Med. Biol. 47 (2002) 123–166.
[12] R. Chen, V. Pagonis, Advances in Physics and Applications of Optically and Thermally Stimulated Luminescence, World Scientific Publishing Europe Ltd, Singapore, 2019.
[13] R. Chen, P.L. Leung, Nonlinear dose dependence and dose-rate dependence of optically stimulated luminescence and thermoluminescence, Radiat. Meas. 33 (2001) 475–481.
[14] J.B. Christensen, M. Togno, K.P. Nesteruk, S. Psoroulas, D. Meer, D.C. Weber, T. Lomax, E.G. Yukihara, S. Safai, Al2O3:C optically stimulated luminescence dosimeters (OSLDs) for ultra-high dose rate proton dosimetry, Phys. Med. Biol. 66 (2021) 085003.
[15] S. Motta, J.B. Christensen, M. Togno, R. Schafer, S. Safai, A.J. Lomax, E. G. Yukihara, Characterization of LiF:Mg,Ti thermoluminescence detectors in low-LET proton beams at ultra-high dose rates, Phys. Med. Biol. 68 (2023) 045017.
[16] L. Karsch, E. Beyreuther, T. Burris-Mog, S. Kraft, C. Richter, K. Zeil, J. Pawelke, Dose rate dependence for different dosimeters and detectors: TLD, OSL, EBT films, and diamond detectors, Med. Phys. 39 (2012) 2447–2455.
[17] C.K. Spindeldreier, O. Schrenk, M.F. Ahmed, N. Shrestha, C.P. Karger, S. Greilich, A. Pfaffenberger, E.G. Yukihara, Feasibility of dosimetry with optically stimulated luminescence detectors in magnetic fields, Radiat. Meas. 106 (2017) 346–351.
[18] E.G. Yukihara, A.J.J. Bos, P. Bilski, S.W.S. McKeever, The quest for new thermoluminescence and optically stimulated luminescence materials: needs, strategies and pitfalls, Radiat. Meas. 158 (2022) 1–19.
[19] E.G. Yukihara, M.F. Ahmed, Pixel bleeding correction in laser scanning luminescence imaging demonstrated using optically stimulated luminescence, IEEE Trans. Med. Imag. 34 (2015) 2506–2517.
[20] E. Bulur, B.E. Saraç, Time-resolved OSL studies on BeO ceramics, Radiat. Meas. 59 (2013) 129–138.
[21] L. Yuan, Y. Jin, Y. Su, H. Wu, Y. Hu, S. Yang, Optically stimulated luminescence phosphors: principles, applications, and prospects, Laser Photon. Rev. 14 (2020) 1–34.
[22] E.G. Yukihara, B.A. Doull, T. Gustafson, L.C. Oliveira, K. Kurt, E.D. Milliken, Optically stimulated luminescence of MgB_4O_7:Ce,Li for gamma and neutron dosimetry, J. Lumin. 183 (2017) 525–532.
[23] T.D. Gustafson, E.D. Milliken, L.G. Jacobsohn, E.G. Yukihara, Progress and challenges towards the development of a new optically stimulated luminescence (OSL) material based on MgB_4O_7:Ce,Li, J. Lumin. 212 (2019) 242–249.
[24] M. Dogan, A.N. Yazici, Thermoluminescence properties of Ce-doped MgB_4O_7 phosphor, J. Optoelectron. Adv. Mater. 11 (2009) 1783–1787.
[25] V.R. Orante-Barrn, L.C. Oliveira, J.B. Kelly, E.D. Milliken, G. Denis, L.G. Jacobsohn, J. Puckette, E.G. Yukihara, Luminescence properties of MgO produced by solution combustion synthesis and doped with lanthanides and Li, J. Lumin. 131 (2011) 1058–1065.
[26] A. Oza, V. Ojha, S. Dhale, S. Dhoble, Photoluminescence and thermoluminescence in Dy^{3+}-, Ce^{3+}-, and Tb^{3+}-activated MgB_4O_7 phosphor for dosimetry application, Luminescence 37 (2022) 1563–1574.
[27] V. Altunal, W. Abusaid, V. Guckan, A. Ozdemir, Z. Yegingil, Luminescence characterization of Ce and Gd doped MgB_4O_7 phosphors, J. Lumin. 246 (2022) 118815.
[28] A. Ozdemir, V. Altunal, V. Guckan, K. Kurt, Z. Yegingil, Luminescence characteristics of newly-developed MgB_4O_7:Ce3+,Na+ phosphor as an OSL dosimeter, J. Alloys Compd. 865 (2021) 158498.
[29] Y. Kitagawa, E.G. Yukihara, S. Tanabe, Development of Ce^{3+} and Li^{+} co-doped magnesium borate glass ceramics for optically stimulated luminescence dosimetry, J. Lumin. 232 (2021) 117847.
[30] M. Bakhsh, W.S. Wan Abdullah, I.S. Mustafa, M.S.A. Al Musawi, N.A.N. Razali, Synthesis, characterisation and dosimetric evaluation of MgB_4O_7 glass as thermoluminescent dosimeter, Radiat. Eff. Defect Solid (2018) 1–15.
[31] V. Pagonis, G. Kitis, Mathematical aspects of ground state tunneling models in luminescence materials, J. Lumin. 168 (2015) 137–144.
[32] L.S.S. Oliveira, L.F. Souza, G.G. Donald, M.F.S. Emidio, A.L.F. Novais, D.N. Souza, Challenges in personal and clinical dosimetry using $Li_2B_4O_7$ and MgB_4O_7 as TLD and OSLD, Brazilian J. Radiat. Sci. 10 (2022) 1–17.
[33] G.F.J. Garlick, A.F. Gibson, The electron trap mechanism of luminescence in sulphide and silicate phosphors, Proc. Phys. Soc. 60 (1948) 574–590.
[34] M.T. Jose, S.R. Anishia, O. Annalakshmi, V. Ramasamy, Determination of thermoluminescence kinetic parameters of thulium doped lithium calcium borate, Radiat. Meas. 46 (2011) 1026–1032.
[35] E.C. Karsu, M. Gökçe, A. Ege, T. Karali, N. Can, M. Prokic, Kinetic characterization of MgB_4O_7: Dy,Na thermoluminescent phosphor, J. Phys. D Appl. Phys. 39 (2006) 1485–1488.